Hindawi
Advances in Civil Engineering
Volume 2023, Article ID 4067940, 14 pages
https://doi.org/10.1155/2023/4067940

*Research Article*

# Torsional Modeling of Reinforced Concrete Beam–Column Joint Retrofitted by Aramid Fiber—Experimental and Numerical Analysis

**Palaniappan Prasath,[1] Ravindran Gobinath ,[2] and Jayaprakash Sridhar [3]**

[1]*Department of Civil Engineering, Muthayammal College of Engineering, Rasipuram, Tamil Nadu, India*
[2]*Department of Civil Engineering, SR University, Warangal 506371, Telangana, India*
[3]*Department of Civil Engineering, GMR Institute of Technology, Rajam, Andhra Pradesh 532127, India*

Correspondence should be addressed to Ravindran Gobinath; gobinathdpi@gmail.com

Received 2 March 2023; Revised 18 August 2023; Accepted 14 September 2023; Published 13 October 2023

Academic Editor: Junqing Zuo



The performance of structural composites during loading has always been a concern for the designers and construction industry since the reinforced concrete structure was discovered. In this study, lateral load–displacement behavior of beam–column joints wrapped with aramid fiber is evaluated using both experimental and numerical analysis subjected to torsional moment (beam-eccentric loading). Three categories of reinforcement concepts are adopted for the preparation of the beam–column joints, where members are wrapped with aramid fiber at the joints, and others are not fortified with aramid fibers. Prior to testing, the structural composites are cured for maximum 28 days into water. The beam–column joints are subjected to lateral load at a point near the column end of the beam–column connection, and the corresponding deflections are measured until the member fails. Based on the test results, ductility and energy absorption capacity are evaluated. The findings of the numerical investigation of beam–column joint show there is not much variation in the experimental and numerical analysis; it is clearly found that aramid fiber wrapping provided large rigidity in the joint, and it is also prolonged the final failure of the joints. This study shows that in addition to the conventional reinforcement, providing the hanger reinforcement and the diagonal reinforcement improves the rigidity of the beam–column joints during severe loadings, as this study described.

## 1. Introduction

Reinforced concrete (RC) structure was indisputably the most adopted construction technology around the world because of the crisis of energy that generated by fossil fuels in 1973. Contractors were forced into leaving to build the steel structure as the cost of conventional steel structures increased too much. Moreover, the population growth and a new construction system, like RC composite structure, was invented at the beginning of the 20th century. However, it had limitations affecting its performance negatively when it was exposed to certain loading, i.e., torsional force. For regular performance development, the concrete composite structure was subjected in harsh assessment condition of in terms of stability, rigidity, deformability, and durability. Plastic rotation, an inelastic twisting of beam and column outside the flexible range, is one of the common deformation types at beam–column joints when it is subjected in lateral loading. In an RC composite structure, the overall performance of the structural framework is majorly dependent on the stability, nondeformability, and rigidity on the beam–column joint. The seismic loading, like earthquake, can negatively influence the performance level of the beam–column joint causing the failure for the entire building skeleton. In real-world scenarios, beams of RC beam–column joints are often subjected to loads that are not perfectly centered. For example, if a building has an irregular layout or if the floor loads are not distributed uniformly, the beams may experience eccentric loads. The application of eccentric loads in these situations can help in simulating real-world conditions, allowing for a more accurate analysis of the behavior of the joint [1]. Concrete reinforced with 1.5% bamboo and 2% jute fibers had a maximum

flexural strength of 6.36 MPa at 28 days of curing [2]. Concrete containing 10% of Posidonia oceanic fibers had a maximum compressive strength of 33.60 MPa, and their thermal conductivity and thermal diffusivity decreased significantly with the addition of fibers [3].

Beam–column joint is an essential connection member in a structural framework, but its failure can cause the collapse of RC composite structure. Also, there is a possibility of disintegration at the joint when concrete composite is fatigued because of spending many years in use. Moreover, during earthquakes, there is a tendency to be physical degradation in the beam–column joint [4, 5]. In such case, the structural composite framework should be modified by retrofitting for member of beam–column joint so that the structure does not encounter the loss on carrying of force and the fatigue. A number of technological steps have been developed which can avoid failure of existing beam–column joint. Longitudinal strengthening bars can be passed through joints to correct dilapidation [6]; however, this procedure can create high shear in the joint center. The use of fibrous materials for retrofitting of concrete composite member shows that the distribution of shear stress in the adhesive layer is substantially impacted by the existence of cracks [7]. Floating fiber-reinforced polymer (FRP) structures for solar panels, FRP composite bumper systems for bridge piers, FRP steel composite piles for foundation applications, and FRP sheets, planks, and piles for modular assembly of a retaining wall are a few examples of how FRP composites are used in the construction of civil infrastructure [8]. The usage of composite rods as a concrete reinforcement material appears to be a viable option to address the durability issues of conventional steel-RC buildings. Several strategies have been developed to prevent corrosion in steel-RC parts [9]. The probability of failure varies for each failure mode in the reliability study for FRP-strengthened RC beams. In order to give a thorough guidance for the design process, it is vital to take into account all potential failure modes [10]. The lateral strength and ductility of the test specimens were greatly enhanced by the addition of carbon fibre reinforced polymer (CFRP) composites to the non-seismic specimen. Particularly, the X-shaped wrapping arrangement, the strips on the column, and the two layers of CFRP sheets produce improved ductility and strength results [11]. The greatest lateral load capacity was achieved by the column-foundation connection reinforced with GFRP bars and CFRP wraps, which is 131.09% higher than that of the control specimen [12]. When compared to externally bonded reinforcement (EBR) joints, anchorage resistance of externally bonded reinforcement on groove (EBROG) joints increased significantly. In using the EBROG approach, no debonding failure in concrete was noticed. It was demonstrated that using the EBROG process for precured CFRP strips resulted in an increase in effective bond length [13]. Increasing in the fiber volume percentage or the use of RC layers at the top, bottom, or throughout the full cross-section of the slabs not only invariably increase slab performance but can also occasionally damage it [14]. Fiber volume ratio has no effect on the mechanical characteristics of the bonding; however, the thickness of the sprayed FRP and the bonding length do. The bonding contact that contributes to shear load carrying may only extend to a certain length before moving from the loaded end to the other end when debonding develops [15]. Double-hooked end steel fiber concretes outperformed single-hooked steel fiber concretes in terms of fracture toughness (12.42 N/m) and fracture energy (955 N/m). Enhancing the fracture resistance of fiber concretes, as well as the effectiveness of size reduction of fiber concrete sections, has been made possible by improved fiber–matrix bonding and alignment of steel fibers along the beam axis [16]. The Young's modulus of the composite will rise with increasing matrix thickness per layer, but it will have an impact on the bridging mechanism of short fibers and lower the hardening modulus and ultimate strength [17, 18] Fiber, like aramid fiber, is obtained from the sources of natural [17], and synthetic [19, 20] with various properties differ from each other.

Aramid fiber, synthetic mac, is also known that it is more durable than that of other conventional fiber as it has weight elevated with quality proportion and highly elastic [21]. The aramid fiber is found that its usage is common in the aviation and military applications due to its high quality of strength though, and it has a lighter weight than that of other conventional fibers. The aramid fiber also has commercial value as it is used for numerous types of applications, i.e., the filament yarns, the staple, the pulp, the chopped fiber composites, and the woven cloth products for special end users [22]. Also, its applications include ballistic-evaluated body defensive layer texture and ballistic composites, bike tires, marine cordage, marine frame support, and substitution of the aramid fiber for asbestos. The aramid fiber is extremely impermeable against the effect of pulling, unlike the carbon nano tube. The application of aramid fiber in a composite also requires epoxy resin treatment to enhance its bonding strength [23]. Epoxy is used as the resin matrix to efficiently hold the fiber in place. It is compatible with all common reinforcing fibers, including fiberglass, carbon fiber, aramid, and basalt. Figure 1 illustrates the aramid fiber, its various usages, and its molecular structure.

Recent advances focus only on a beam element in the use of aramid fiber for strengthening concrete composite structures [21, 24, 25]; however, as the studies have a limit on the repairing in a single composite member, it may not prevent total collapse in a concrete composite structure. Concrete cube double-wrapped with aramid fibers increases the compressive strength by 140% at room temperature and 150% when dried in an oven at 200°C [26]. RC beams shear strengthened with aramid fibers have good strength when compared with unconfined beams in both wrapping and single and double piles [27]. Beam–column joint containing high-performance fibers reinforced cementitious composites exhibits flexural failure rather than shear failure in the case of nonseismic detailed specimen [28]. The beam–column joints provided with steel fibers exhibit higher ductility, energy absorption, and stiffness when compared to conventional RC beam–column joints [29]. Beam–column joint with reactive powdered concrete under static load improve the load carrying capacity by 32% and first crack load by 60% when compared with beam–column joints with normal concrete [30]. In finite

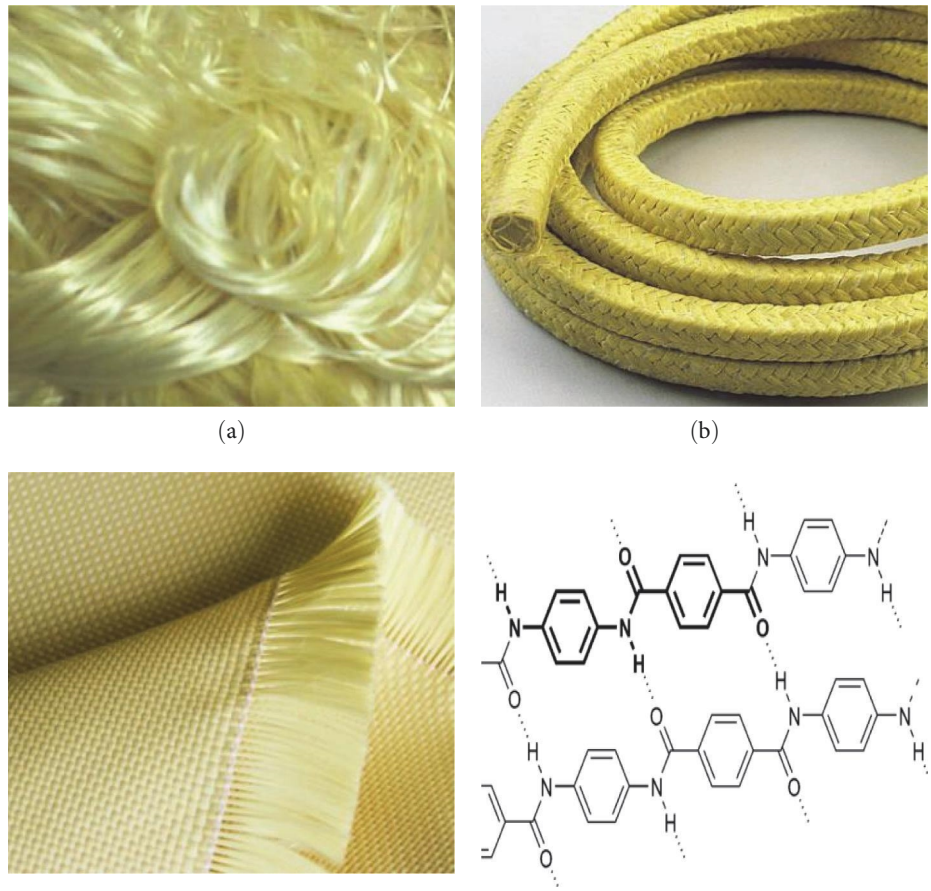

(a) (b) (c) (d)

Figure 1: The aramid fiber: (a) raw fiber; (b) pipe; (c) fabric; (d) molecular structure.

Table 1: Physical properties of aggregates.

| Types of aggregate | Properties | | | | | |
|---|---|---|---|---|---|---|
| | Specific gravity ($g/cm^3$) | Water absorption (%) | Fineness modulus (%) | Aggregate impact value (%) | Elongation (%) | Flakiness index (%) |
| River sand | 2.68 | 1 | 2.8 | – | – | – |
| Granite | 2.66 | 2 | – | 38.73 | 16.68 | 14.29 |

element modeling, using Abaqus for RC beam–column joint indicates that the use of different sizes of mesh and values for the viscosity led to decreased analysis time and fewer analysis steps. This research introduces a novel modeling technique involving reactive powder concrete beam–column joints for predicting structural behavior and response. It also aims to enhance shear strength resistance against various structural loads [31]. In beam–column joint, the headed bars have the advantage of improving a much wider compressive strength in the joint, along with joint confinement, which improves the joint's overall performance. They also have the advantage of transferring a more uniform distribution of compressive stress to the concrete at the headed end [32, 33]. The beam–column junction specimens without joint hoop reinforcement experience significant displacement and develop broader cracks. The ultimate load-carrying capacity, energy dissipation, displacement ductility, and joint shear strength all rise with an increase in joint hoop reinforcement [32, 33].

Therefore, in the current study, the lateral displacement–load behavior of beam–column joint wrapped with the aramid fiber is evaluated with focusing on the experimental and numerical analysis. The present study is a significant key as its results tend to be useful for fixing the joint structurally in the distressed concrete composite structure affected by surplus loadings such as earthquakes and landslides.

## 2. Materials and Methods

*2.1. Materials, Properties, and Mix Proportions.* The objective of this study is to investigate the behavior of beam–column joint that is wrapped with aramid fiber. A concrete mix grade of M30 was designed for casting the beam–column members.

Table 2: Mix proportions.

| Type of mixture | Materials | | | |
|---|---|---|---|---|
| | Cement (kg/m$^3$) | River sand (kg/m$^3$) | Granite (kg/m$^3$) | Water/cement ratio |
| Ratio | 1 | 2.05 | 2.52 | 0.47 |
| Proportion | 394 | 803 | 992 | 0.47 |

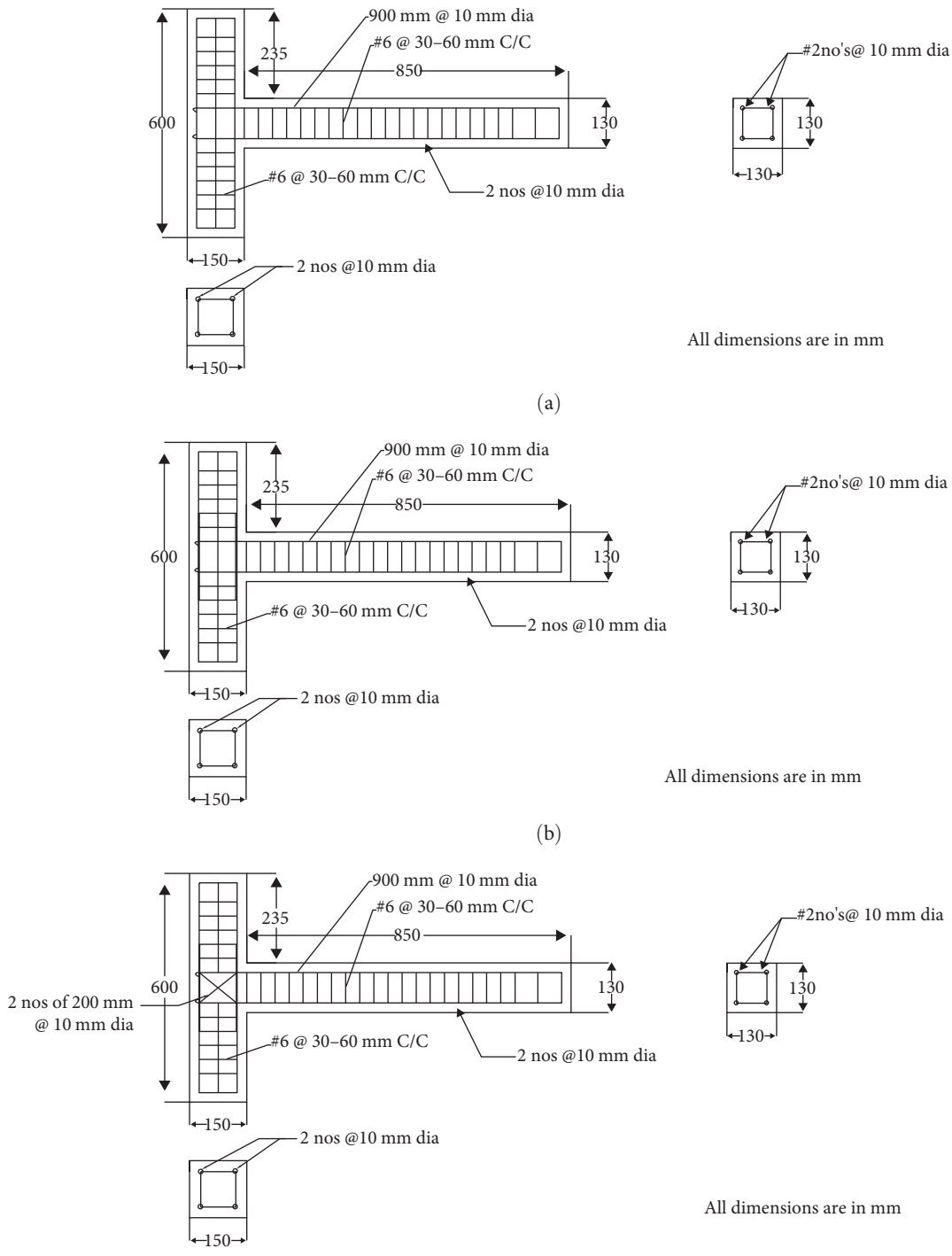


Figure 2: Reinforcement arrangement: (a) A-type; (b) B-type; (c) C-type.

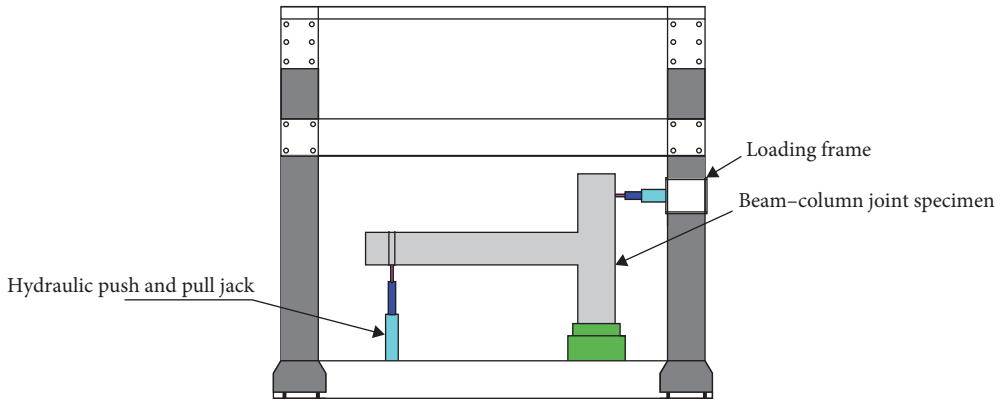


Figure 3: Schematic diagram of test setup.

Table 3: The parameters used for modeling of the aramid fiber reinforced concrete composite structure in the Abaqus software.

| Properties | Types of material | | |
|---|---|---|---|
| | Concrete | Aramid fiber | Reinforcing steel bar |
| Density (kg/m$^3$) | 2,400 | 1,450 | 7,850 |
| Compressive strength (MPa) | 29 | – | – |
| Splitting tensile strength (MPa) | 3.9 | – | – |
| Flexural strength (MPa) | 0.11 | – | – |
| Modulus of elastic (MPa) | 19,364 | 90,000 | 210,000 |
| Poison's ratio | 0.17 | 0.36 | 0.27 |
| Characteristic strength (MPa) | 30 | – | – |
| Yield strength (MPa) | – | 3,000 | 415 |

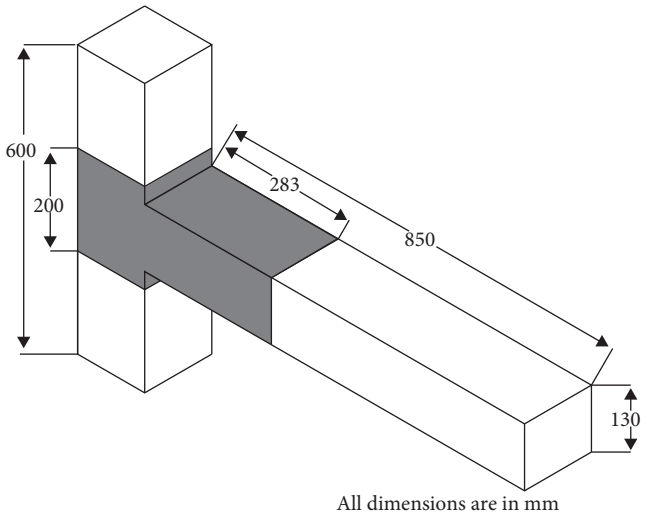


Figure 4: Wrapping of aramid fibers.

The materials used for the experiment include granite as coarse aggregate, natural river sand as fine aggregate, ordinary Portland cement, and aramid fiber. The properties of the aggregates determined include specific gravity, flakiness and elongation, water absorption, impact value, crushing strength, abrasion resistance, attrition resistance, and fineness

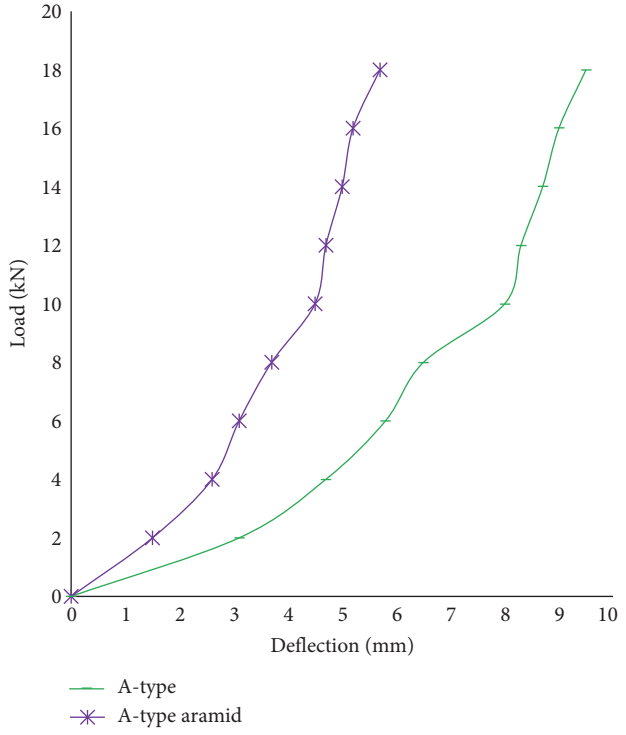


Figure 5: Load-deflection of beam–column member A-type and A-type with aramid fiber.

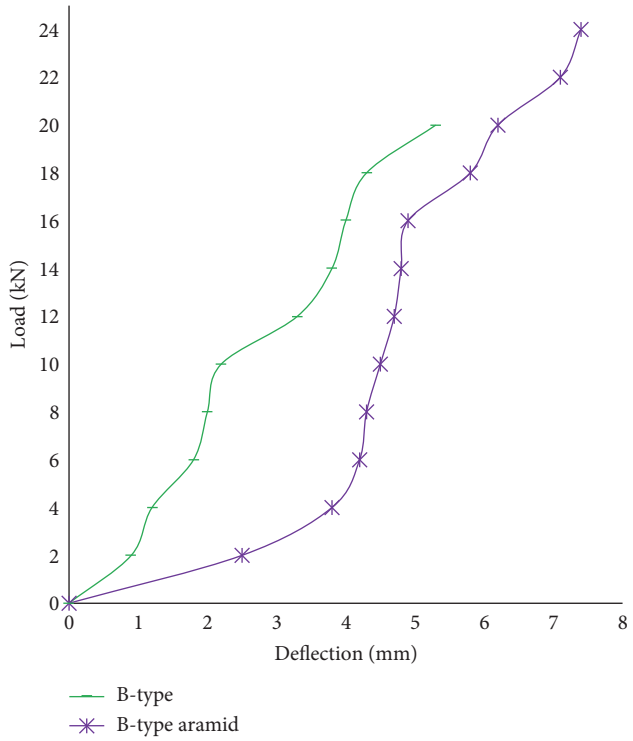


Figure 6: Load-deflection of beam–column member B-type and B-type with aramid fiber.

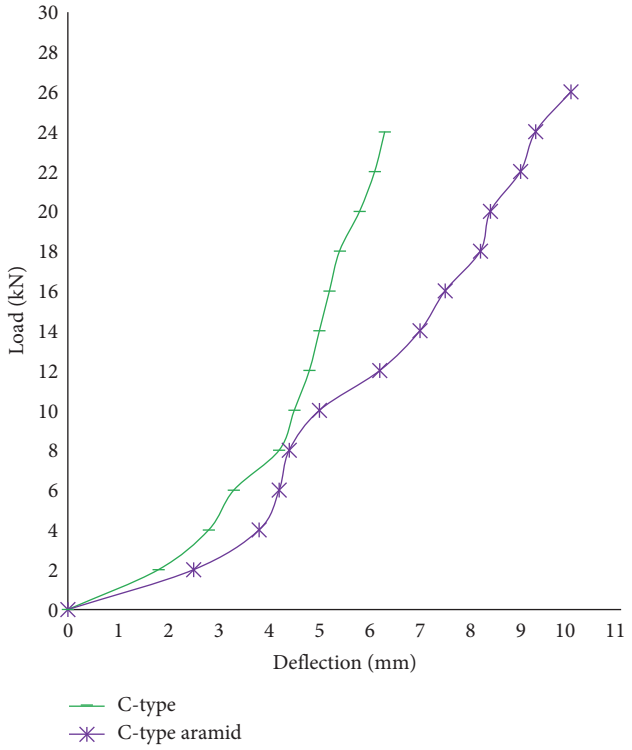


Figure 7: Load-deflection of beam–column member C-type and C-type with aramid fiber.

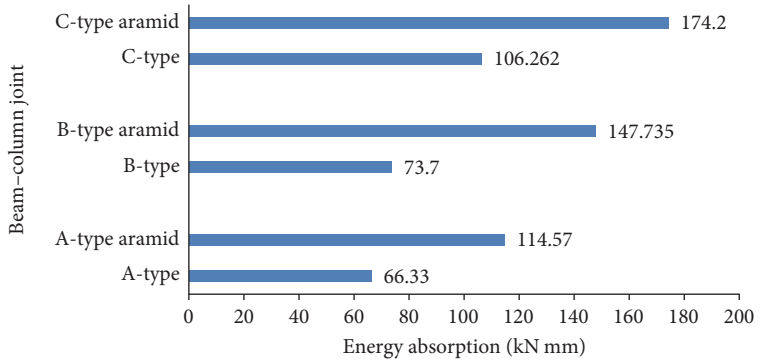


Figure 8: Energy absorption of beam–column joints.

modulus. The aggregate properties were determined according to the procedures in Indian standards (IS 2386-3, 1963 [34]), and cement tests were done following IS 4031 [35]. The coarse aggregate was of size ranges 12–20 mm, and fine aggregate was the portion of the material that passed 4.75 mm aperture size. Aramid fiber was recycled in a bullet-resistance jacket. This fiber had good abrasive resistance, and under repeated loading, they can scratch against each other by weakening the sheets. The aramid fiber was prepared from synthetic products and characterized by strength. The thickness of the aramid fiber was 1.5 mm, and overall size was $4.0 \times 1.2$ m. The density of aramid fiber was 1.44 g/cm$^3$ and elongation was 2.8%. Table 1 gives the properties of the aggregates, and Table 2 presents the mix proportions.

*2.2. Experimental and Numerical Modeling.* Six types of beam–column joints were investigated; A-type, which had the conventional reinforcement arrangement (Figure 2(a)), B-type, where hanger bars are added at the joint (Figure 2(b)), C-type (Figure 2(c)), where diagonal cross bars and hanger bars are added at the joint, and the remaining three members include A-type, B-type, and C-type wrapped with aramid fiber. Beam–column joint with cross-sectional dimension of beam of $130 \times 130$ mm, length of beam 1,000 mm were employed. Column with cross-section $150 \times 150$ mm and length 600 mm were adopted.

Figure 3 shows the of load setup for the beam–column joint during the experimental investigation. When the member has been positioned in a loading frame of 2,000 (kN)

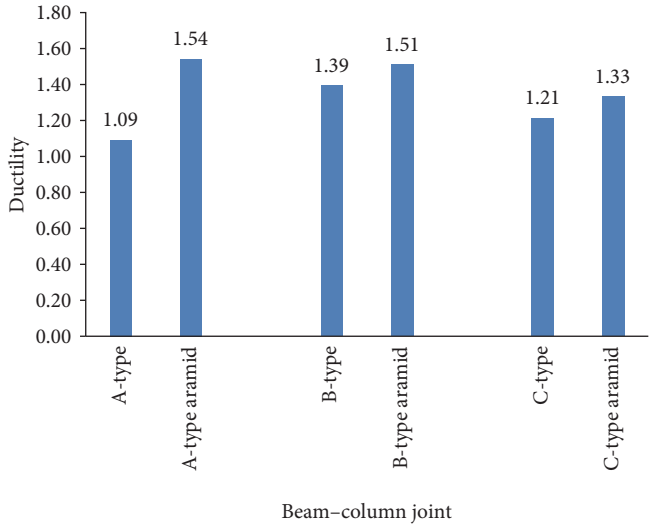


Figure 9: Ductility of beam–column joint.

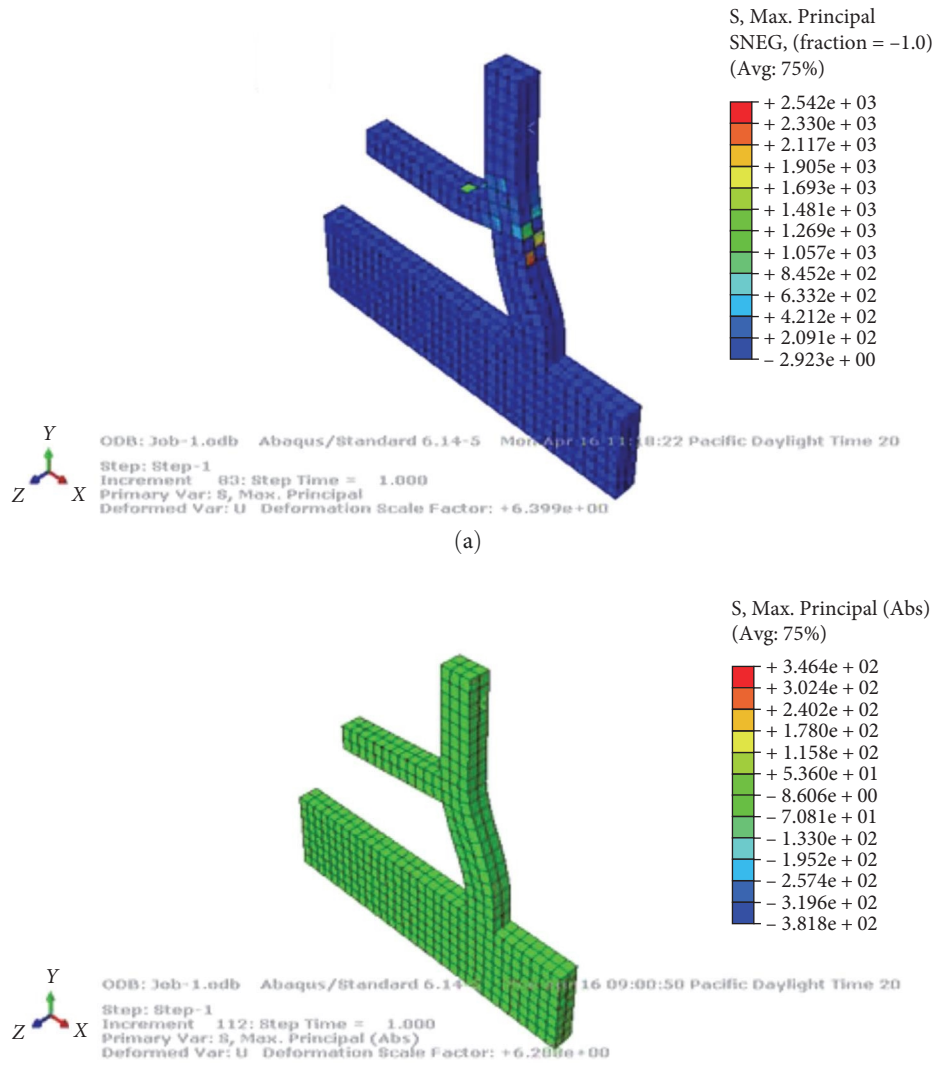


Figure 10: Maximum principal stress: (a) A-type without aramid fiber; (b) A-type with aramid fiber.

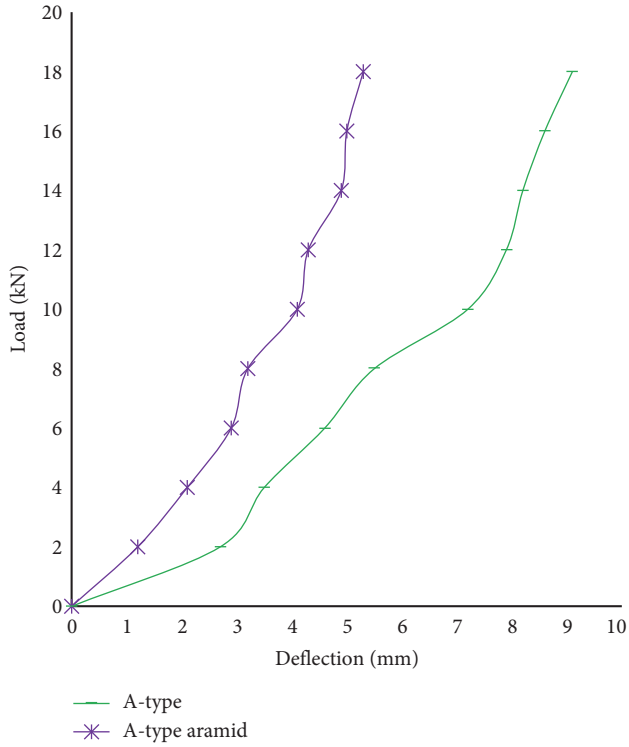


Figure 11: Analytical Load versus displacement for A-type member without aramid fiber and with aramid fiber.

capacity, then the load was applied near one end of the column. To measure the applied load, load cell of capacity 500 kN was used. The deflection of the member was measured on the dial gauge attached to the machine. Resulting cracks propagation at the beam–column joint were observed and marked. The yield point in the RC beam–column joint is recorded by crack observation method. Incremental loads are applied to the joint specimen, and observations are made for the formation of cracks in the concrete. At the yield point, formation of wider and more visible cracks will be noticed, indicating the onset of plastic deformation. The behavior of beam–column joints was also explored using the finite element approach. The numerical simulation and analysis were performed in Abaqus finite element software in order to study the behavior of the beam–column joints under loading. Table 3 gives the parameters used for modeling of the aramid fiber RC composite structure in the Abaqus software.

*2.3. Retrofitting Process.* The specimens' surfaces were meticulously cleaned. The surface where aramid fibers to be wrapped was covered with a very thin layer of resin that had been well mixed with the hardener. The surface was then covered with the aramid fiber that had been trimmed to size. The cloth was bonded onto the surfaces as distinct sections covering the sides of the beam and columns by wrapping around in one layer. Any air voids that had been caught in the interface were removed by rolling a small hand roller over the fastened fabric. For 24 hr, the specimens were held at room temperature to verify that the fibers were completely bonded. The illustration of fiber wrapping can be seen in Figure 4.

## 3. Results and Discussions

*3.1. Experimental Evaluation.* During the loading of the column end of the beam–column connections, the resulting load, and deflection on the member were measured. Figure 5 shows the load-deflection plot for A-type joint without aramid fiber and A-type with aramid fiber, respectively. The load-deflection behavior was linear upto the first crack load. For the member without aramid fiber, the ultimate load of specimen was 18 kN at a deflection of 9.3 mm. The initial crack occurred at 14 kN and deflection of 8.7 mm. Whereas, when aramid fiber had been applied to the A-type beam–column joint, the ultimate load of specimen was 18 kN at a deflection of 5.7 mm. The initial crack occurred at 8 kN at a deflection of 3.7 mm. With this result, there was a significant strengthening effect of aramid fiber on the A-type member, which resulted in limited deformation experienced in members with aramid fiber. The higher stiffness of aramid fiber helps the flexural rigidity around the joint of the beam–column connection. This observation agrees with the finding of a similar study [36], which reported that aramid fiber enhanced the bending strength of beams.

Figure 6 shows the load-deflection plot for B-type without aramid fiber and B-type with aramid fiber, respectively. For the member without aramid fiber, the ultimate load of specimen was 20 kN at a deflection of 5.4 mm. The initial crack occurred at 14 kN and deflection of 3.8 mm. Whereas, when aramid fiber had been applied to the B-type beam–column joint, the ultimate load of specimen was 24 kN at a deflection of 7.5 mm. The initial crack occurred at 16 kN at a deflection of 4.9 mm. With this result, there was a significant strengthening

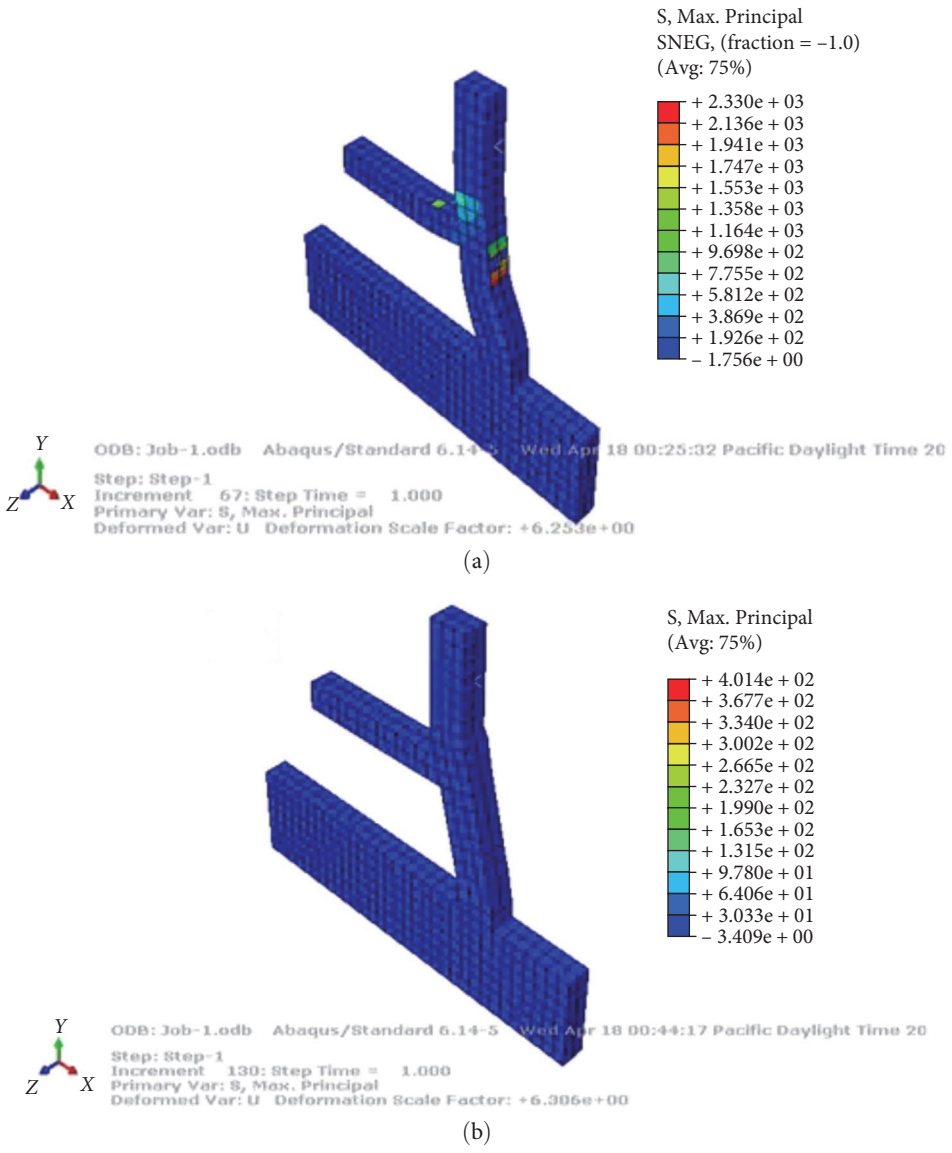


Figure 12: Maximum principal stress: (a) B-type without aramid fiber; (b) B-type with aramid fiber.

effect of aramid fiber on the B-type member due to limited deformation experienced in members with aramid fiber.

Figure 7 shows the load-deflection plot for C-type without aramid fiber and C-type with aramid fiber, respectively. For the member without aramid fiber, the ultimate load of specimen was 24 kN at a deflection of 6.4 mm. The initial crack occurred at 16 kN and deflection of 5.2 mm. Whereas, when aramid fiber had been applied to the C-type beam–column joint, the ultimate load of specimen was 26 kN at a deflection of 10.1 mm. The initial crack occurred at 16 kN at a deflection of 7.5 mm. With this result, there was a significant strengthening effect of aramid fiber on the C-type member due to limited deformation experienced in members with aramid fiber. Moreover, the initial crack appeared later than in members without aramid fiber and was equivalent to that beam normally designed for lateral loads. As such, it can be said that the use of aramid fiber controlled the propagation of cracks.

Energy absorption is the area under the load–deflection curve. The energy absorption capacity of specimens is manifested in Figure 8. From the figure, it is clear that maximum energy absorption of 174.2 kN mm was obtained for C-type beam–column joint wrapped with aramid fibers. Similarly, for A-type and B-type beam–column joints wrapped with aramid fibers, energy absorption was obtained as 114.57 and 147.735 kN mm, respectively.

Ductility is a crucial property of an RC beam–column joint, especially in seismic regions, as it allows the joint to absorb energy and undergo significant deformations without sudden failure. In the current investigation, ductility is determined by using load–deflection curve. Ductility is often calculated by comparing the ultimate displacement or deformation to the yield point displacement. From the load–deflection response, ductility is arrived, which is assumed as bilinear. The ductility factor can be calculated as the ratio of ultimate deformation to

yield deformation. The ductility of beam–column joints is arrayed in Figure 9. The maximum ductility of A-type aramid beam–column joint was found to be 1.54, whereas the maximum ductility of 1.51 was obtained for B-type beam–column joint. Similarly, for C-type aramid beam–column joint, ductility was found to be 1.33. In all the cases, the ductility is maximum for wrapped beam–column joints.

### 3.2. Numerical Evaluation

*3.2.1. Constitutive Models and Material Properties.*

*(1) Concrete* Numerous constitutive models that can forecast concrete behavior, such as cracks and crushing, have been created in recent years. Concrete behavior can be predicted using two methods in Abaqus: smeared crack and plastic damage models. Since the plastic damage model has a larger potential for convergence than the smeared crack model, it has been chosen for this study with element type C3D8R. The two primary concrete failure mechanisms are assumed by the concrete, plastic damage model to be crushing and cracking. The elastic modulus, Poisson's ratio, plastic damage parameters, and descriptions of compressive and tensile behavior are needed for the plastic damage model. The dilation angle, flow potential eccentricity, initial equibiaxial compressive yield stress to initial uniaxial compressive yield stress, second stress invariant on the tensile meridian to that on the compressive meridian, and the viscosity parameter that determines viscoplastic regularization are the five parameters that determine plastic damage [31, 37].

*(2) Steel Reinforcement* The conventional metal elastic-perfectly plastic model with T3D2 element was utilized as the constitutive model to represent the steel reinforcement. The assumption has been made that steel is an elastic, perfectly pliable substance that responds to stress and compression equally. The elastic modulus, Poisson's ratio, and the yield stress are the inputs for the steel model. In the experimental investigation, the elastic modulus, Es, and yield stress, fy, were measured. The results showed that Es = 210 GPa, fy = 415 MPa, and the Poisson's ratio was taken to be 0.27.

*(3) Aramid Fibers* As a linear elastic orthotropic material with an S4R element, the aramid fiber was modeled. It is clear that the behavior is primarily orthotropic because the composite is unidirectional. Manufacturer specifications for the unidirectional aramid fiber material utilized in the experimental study state that its elastic modulus in the fiber direction is 90 GPa and its Poisson ratio is 0.3. The isotropic model uses this value for $E$ and $v = 0.3$.

*(4) Interface between Concrete and Aramid Fiber* It is very important to have a model for the aramid fiber and concrete contact. This research assumes a perfect connection at the concrete and aramid fiber contact.

*(5) Boundary Conditions and Meshing* Based on calibration using existing experimental data, the ideal mesh size was identified (i.e., this mesh best reproduces experimental data). Modeling reinforcement bars utilized 2-noded single Gauss point truss elements that were placed to match the specimens' detailing of the reinforcement (such as bar spacing, cover distance, etc.). A fixed boundary condition is adopted such that the top end of the column is rigidly attached and it is fixed in space. This would mean that the displacement and rotation of the top end of the column are both constrained in all directions [38].

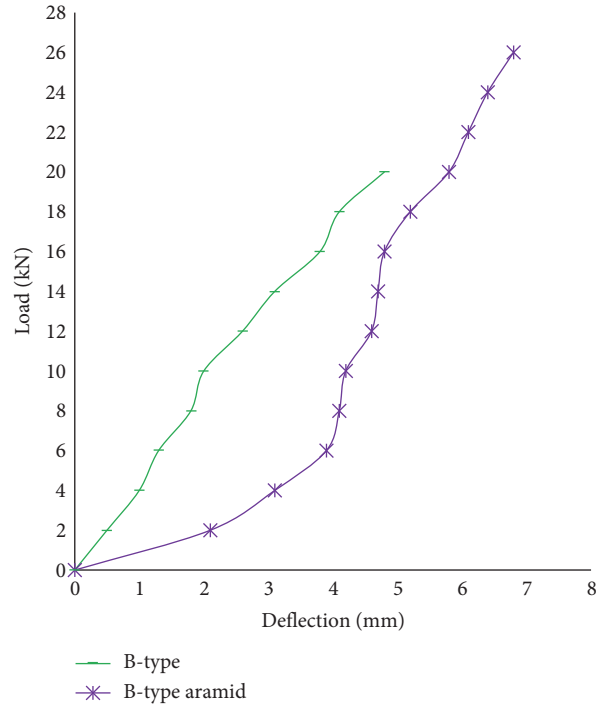


Figure 13: Load versus displacement for B-type member without aramid fiber and with aramid fiber.

The analysis of all types of the beam–column joints has been performed in Abaqus finite element software. Figures 10(a) and 10(b) show the maximum principal stress of A-type beam–column joint. In the member without aramid fiber, the maximum principal stress was found to be $2.542 \times 10^{-2}$ N/mm$^2$. While A-type member with aramid fiber had maximum principal stress of $3.646 \times 10^{-2}$ N/mm$^2$. The load-deflection plots for the A-type beam–column joint with and without aramid fiber are presented in Figure 11. As can be seen from the Figures, the ultimate load for A-type beam–column joint is 18 kN, and the corresponding deflection is 9.1 mm. Similarly for A-type aramid fiber beam–column joint ultimate load was 18 kN and corresponding deflection was 5.3 mm. The beam–column joint with aramid fiber had prolonged resistance to loading than in the member without aramid fiber.

The maximum principal stress obtained for the B-type beam–column joint is presented in Figure 12. The member with aramid fiber developed higher stress than the joint without aramid fiber (Figures 12(a) and 12(b)). In the member without aramid fiber, the maximum principal stress was found to be $2.330 \times 10^{-2}$ N/mm$^2$. Whereas B-type member with aramid fiber had a maximum principal stress of $4.014 \times 10^{-2}$ N/mm$^2$. The load-deflection plots for the B-type beam–column joint with and without aramid fiber are presented in Figure 13. As can be seen from the following figures, the ultimate load obtained from B-type beam–column joint is 20 kN, and the corresponding deflection is 4.8 mm. Similarly, the ultimate load for B-type aramid beam–column joint is 26 kN, and the corresponding deflection is 6.8 mm.

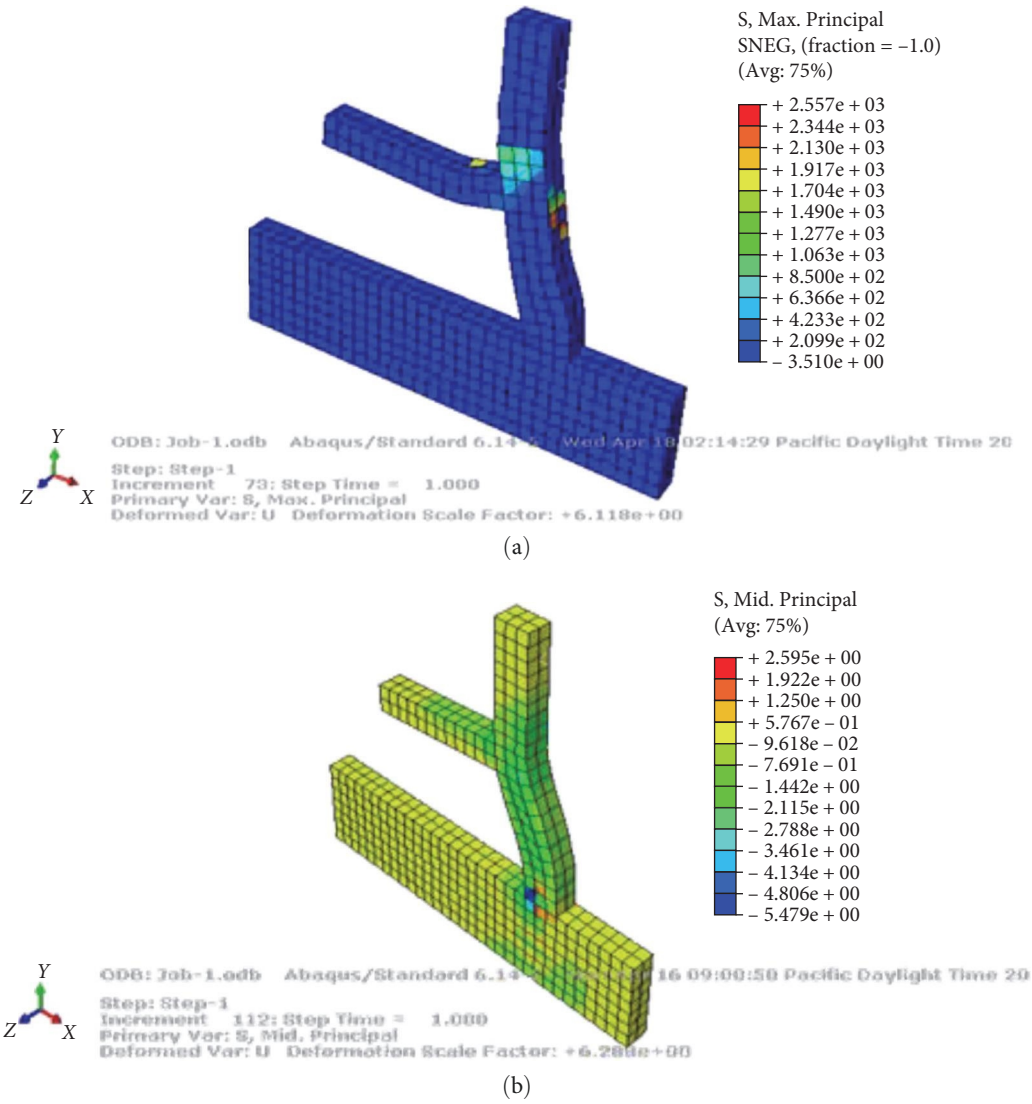


Figure 14: Maximum principal stress: (a) C-type without aramid fiber; (b) C-type with aramid fiber.

Figures 14(a) and 14(b) show the maximum principal stress obtained for the C-type beam–column joint. The member with aramid fiber developed higher stress than the joint without aramid fiber. In the member without aramid fiber, the maximum principal stress was found to be $2.557 \times 10^{-2}$ N/mm$^2$. Whereas C-type member with aramid fiber had a maximum principal stress of $2.595 \times 10^{-2}$ N/mm$^2$. The load-deflection plots for the C-type beam–column joint with and without aramid fiber are presented in Figure 15. As can be seen from the following figures, the ultimate load for C-type beam–column joint is 26 kN, and the corresponding deflection is 6.5 mm. Similarly, the C-type beam–column joint with aramid fibers is 28 kN, and the corresponding deflection is 8.2 mm.

From the experimental and numerical analysis, aramid fiber was found to practically make a difference by improving the rigidity and resistance of beam–column joints to lateral failures. The behavior of the beam–column joints under the experimental and numerical analysis in Abaqus software are somewhat similar. The aramid strengthened joints demonstrated a huge tendency to resist twisting loads. Correlation with the quantity of aramid fiber wrapped with the increase in load capacity is arrayed in Table 4. From the table, it is clear that for each type (A-type aramid, B-type aramid, and C-type aramid) is wrapped with one layer, which is about 0.2 m$^2$. A-type aramid beam–column joint has the same ultimate load of 18 kN when compared to an unwrapped A-type beam–column joint. In the case of B-type aramid beam–column joint, the ultimate load increases by 20% when compared to an unwrapped specimen. Similarly, in the case of C-type aramid beam–column joint, the ultimate load increases by 8.3%. Based on these results, it would be appropriate that aramid fibers increase the strength, stiffness, and durability and an effective technique for enhancing their performance and extending their service life. Comparison of experimental and analytical investigation are shown in Table 5.

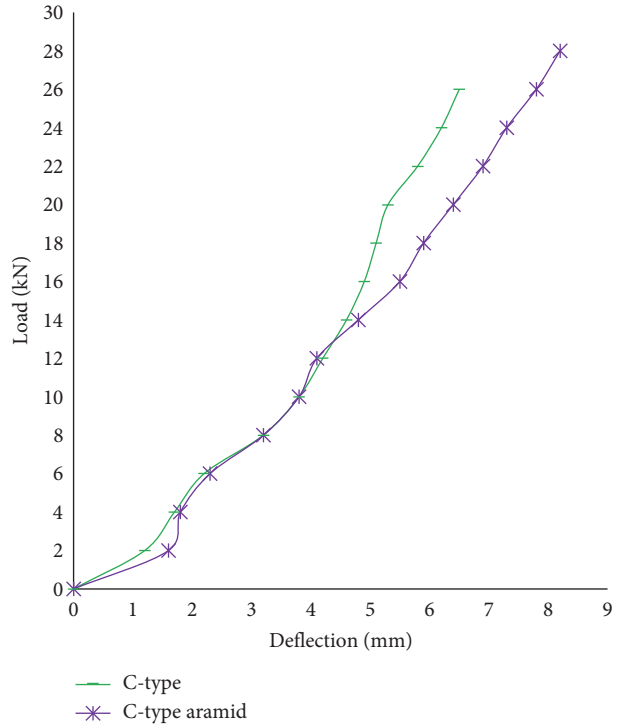


Figure 15: Load versus displacement for C-type member without aramid fiber and with aramid fiber.

Table 4: Correlation of quantity of aramid fibers with ultimate load.

| Beam–column joint | Wrapped/unwrapped | No of layers | Quantity of aramid fibers ($m^2$) | Ultimate load (kN) | Increase in ultimate load (%) |
|---|---|---|---|---|---|
| A-type | Unwrapped | – | | 18 | – |
| A-type aramid | Wrapped | 1 | 0.2 | 18 | 0 |
| B-type | Unwrapped | – | | 20 | – |
| B-type aramid | Wrapped | 1 | 0.2 | 24 | 20 |
| C-type | Unwrapped | – | | 24 | – |
| C-type aramid | Wrapped | 1 | 0.2 | 26 | 8.34 |

Table 5: Comparison of experimental and finite element analysis.

| Beam–column joint | FCL (kN) | | $FCL_\partial$ (mm) | | UL (kN) | | $UL_\partial$ (mm) | |
|---|---|---|---|---|---|---|---|---|
| | Exp | Abaqus | Exp | Abaqus | Exp | Abaqus | Exp | Abaqus |
| A-type | 14 | 13 | 8.7 | 8.3 | 18 | 18 | 9.3 | 9.1 |
| A-type aramid | 8 | 8 | 3.7 | 3.6 | 18 | 18 | 5.7 | 5.3 |
| B-type | 14 | 14 | 3.8 | 3.7 | 20 | 20 | 5.4 | 4.8 |
| B-type aramid | 16 | 16 | 4.9 | 5.0 | 24 | 26 | 7.5 | 6.8 |
| C-type | 16 | 15 | 5.2 | 5.1 | 24 | 26 | 6.4 | 6.5 |
| C-type aramid | 16 | 16 | 7.5 | 7.5 | 26 | 28 | 10.1 | 8.2 |

*Note*: FCL, first crack load; $FCL_\partial$, ultimate load; UL, ultimate load; $UL_\partial$, ultimate load deflection.

## 4. Conclusions

This study evaluates the lateral displacement-load behavior of beam–column joints which have been wrapped with aramid fiber using experimental and numerical analysis. Beam–column joints under three categories of reinforcement arrangements were subjected to lateral loading towards the column end, after which the load and deflection at the joints were determined. The following conclusions were drawn from the study:

(i) There was a significant impact provided by the aramid fiber on the resistance of the beam–column joints to loading. Although reinforcement arrangement also contributed to the member's behavior,

but the aramid fiber possesses the ability to increase the rigidity of joints.

(ii) The ultimate load of the A-type beam–column joint without aramid fiber was 18 kN with a deflection of 9.5 mm, whereas the joints with aramid fiber had wrapping had a deflection of 5.7 mm. Thus, aramid fibers reduce the deflection in A-type beam–column joint by 40% when compared to unwrapped A-type beam–column joint.

(iii) In B-type with aramid and C-type aramid fiber beam–column joint, the ultimate load was found to be 24 and 26 kN, respectively, which is 16% and 7% higher than unwrapped beam–column joints. This is due to the high tensile strength and stiffness of aramid fibers, which can help to distribute the loads more evenly across the structure.

(iv) The energy absorption of A-type aramid wrapped, B-type aramid, and C-type aramid-wrapped beam–column joint is about 39%, 50%, and 42% higher than unwrapped beam–column joints.

(v) The ductility of A-type aramid wrapped, B-type aramid, and C-type aramid-wrapped beam–column joint is about 39%, 8%, and 9% higher than unwrapped beam–column joints.

(vi) The load–deflection results obtained from the numerical investigation is very close to the load–deflection curve obtained from the experimental study. The ultimate load obtained in numerical investigation goes in hand with experimental study.

(vii) The C-type beam–column joint, having conventional reinforcement combined with hanger bars and diagonal reinforcements, gave the best resistance to joint failure. Also, the beam–column joint was well strengthened by using aramid fiber wrapping at joint. The ultimate load of the C-type beam–column joint without aramid fiber wrapping was 24 and 26 kN for the joints with aramid fiber wrapping at 28 days.

(viii) The use of aramid fibers can also help to reduce the cracking and deformation of RC beam–column joints, which can lead to a longer service life for the structure. This is due to the high modulus of elasticity and low creep of aramid fibers, which can help to maintain the integrity of the structure over time and make them as cost-effective and reliable solution for improving the performance and durability of concrete structures.

## Data Availability

The "Experimental and Numerical Research" data used to support the findings of this study are available from the corresponding author upon request.

## Disclosure

Authors declare that this study did not include any research budget obtained from either nonprofit organizations and/or profit organizations.

## Conflicts of Interest

The authors declare that they have no conflicts of interest.

## References

[1] J. Y. R. Liew, W. F. Chen, and H. Chen, "Advanced inelastic analysis of frame structures," *Journal of Constructional Steel Research*, vol. 55, no. 1–3, pp. 245–265, 2000.

[2] J. Sridhar, R. Gobinath, and M. S. Kırgız, "Comparative study for efficacy of chemically treated jute fiber and bamboo fiber on the properties of reinforced concrete beams," *Journal of Natural Fibers*, vol. 19, no. 15, pp. 12224–12234, 2022.

[3] O. Benjeddou, M. Jedidi, M. A. Khadimallah, G. Ravindran, and J. Sridhar, "Effect of *Posidonia oceanica* fibers addition on the thermal and acoustic properties of cement paste," *Buildings*, vol. 12, no. 7, Article ID 909, 2022.

[4] M. F. M. Fahmy, "Advanced fiber-reinforced polymer (FRP) composites to strengthen structures vulnerable to seismic damage," in *Advanced Fibre-Reinforced Polymer (FRP) Composites for Structural Applications*, pp. 511–551, Woodhead Publishing, 2013.

[5] J. Shafaei, A. Hosseini, M. S. Marefat, J. M. Ingham, and H. Zare, "Experimental evaluation of seismically and non-seismically detailed external RC beam–column joints," *Journal of Earthquake Engineering*, vol. 21, no. 5, pp. 776–807, 2017.

[6] H. Rodrigues, P. M. Pradhan, A. Furtado, P. Rocha, and N. Vila-Pouca, "Structural repair and strengthening of RC elements with concrete jacketing," in *Strengthening and Retrofitting of Existing Structures*, pp. 181–198, Springer, Singapore, 2018.

[7] T. Ayad, T. Kadri, and A. Rezigua, "Mechanical behavior after repairing structure by fiber carbon," *Revista de La Construcción. Journal of Construction*, vol. 16, no. 3, pp. 412–419, 2017.

[8] H. Fang, Y. Bai, W. Liu, Y. Qi, and J. Wang, "Connections and structural applications of fibre reinforced polymer composites for civil infrastructure in aggressive environments," *Composites Part B: Engineering*, vol. 164, pp. 129–143, 2019.

[9] R. Fangueiro and C. Gonigho-Pereira, "Fibrous materials reinforced composite for internal reinforcement of concrete structures," in *Fibrous and Composite Materials for Civil Engineering Applications*, pp. 216–249, Woodhead Publishing, 2011.

[10] X. Huang, L. Sui, F. Xing, Y. Zhou, and Y. Wu, "Reliability assessment for flexural FRP-strengthened reinforced concrete beams based on importance sampling," *Composites Part B: Engineering*, vol. 156, pp. 378–398, 2019.

[11] K. Le-Trung, K. Lee, J. Lee, D. H. Lee, and S. Woo, "Experimental study of RC beam–column joints strengthened using CFRP composites," *Composites Part B: Engineering*, vol. 41, no. 1, pp. 76–85, 2010.

[12] M. Miralami, M. R. Esfahani, and M. Tavakkolizadeh, "Strengthening of circular RC column-foundation connections with GFRP/SMA bars and CFRP wraps," *Composites Part B: Engineering*, vol. 172, pp. 161–172, 2019.

[13] N. Moshiri, A. Tajmir-Riahi, D. Mostofinejad, C. Czaderski, and M. Motavalli, "Experimental and analytical study on CFRP strips-to-concrete bonded joints using EBROG method," *Composites Part B: Engineering*, vol. 158, pp. 437–447, 2019.

[14] M. G. Naghibdehi, M. K. Sharbatdar, and M. Mastali, "Repairing reinforced concrete slabs using composite layers," *Materials & Design*, vol. 58, pp. 136–144, 2014.

[15] Z. Yang and J. Li, "Double shear test on bonding mechanical properties of sprayed FRP and concrete substrate," *Composites Part B: Engineering*, vol. 162, pp. 388–396, 2019.

[16] S. Anandan, S. Islam, and R. Abad, "Characteristics of steel fibre reinforced high strength concrete beams: efficiency in size reduction for flexure," *Engineering Journal*, vol. 22, no. 4, pp. 191–208, 2018.

[17] B. Li, H. Xiong, J. Jiang, and X. Dou, "Tensile behavior of basalt textile grid reinforced engineering cementitious composite," *Composites Part B: Engineering*, vol. 156, pp. 185–200, 2019.

[18] Z. Zheng and D. Feldman, "Synthetic fibre-reinforced concrete," *Progress in Polymer Science*, vol. 20, no. 2, pp. 185–210, 1995.

[19] S. S. Mir, S. M. N. Hasan, M. J. Hossain, and M. Hasan, "Chemical modification effect on the mechanical properties of coir fiber," *Engineering Journal*, vol. 16, no. 2, pp. 73–84, 2012.

[20] S. Thirumurugana and S. Anandan, "Residual strength characteristics of polymer fibre concrete exposed to elevated temperature," *Engineering Journal*, vol. 19, no. 4, pp. 117–131, 2015.

[21] S. B. Kandekar and R. S. Talikoti, "Torsional behaviour of reinforced concrete beams retrofitted with aramid fiber," *Advances in Concrete Construction*, vol. 9, no. 1, pp. 1–7, 2020.

[22] M. Ertekin, "Aramid fibers," in *Fiber Technology for Fiber-Reinforced Composites*, pp. 153–167, Woodhead Publishing, 2017.

[23] T.-M. Liu, Y.-S. Zheng, and J. Hu, "Surface modification of aramid fibers with new chemical method for improving interfacial bonding strength with epoxy resin," *Journal of Applied Polymer Science*, vol. 118, no. 5, pp. 2541–2552, 2010.

[24] S. Hong and S.-K. Park, "Behavior of concrete beams with peel-plied aramid-fiber-reinforced polymer plates," *Mechanics of Composite Materials*, vol. 52, pp. 43–54, 2016.

[25] K. Shen, S. Wan, Y. L. Mo, and Z. Jiang, "Theoretical analysis on full torsional behavior of RC beams strengthened with FRP materials," *Composite Structures*, vol. 183, pp. 347–357, 2018.

[26] R. S. Talikoti and S. B. Kandekar, "Strength and durability study of concrete structures using aramid-fiber-reinforced polymer," *Fibres*, vol. 7, no. 2, Article ID 11, 2019.

[27] J. S. Ruben, M. Murugan, and J. P. A. Jose, "The effect of aramid fibre reinforced polymer composites for strengthening RC beams," *Journal of Fiber Science and Technology*, vol. 76, no. 10, pp. 343–350, 2020.

[28] W. Nadir, A. Y. Ali, and M. M. A. Kadhim, "Structural behavior of hybrid reinforced concrete beam–column joints under cyclic load: state of the art review," *Case Studies in Construction Materials*, vol. 15, Article ID e00707, 2021.

[29] P. Pooja, V. Girija, K. Vidhya, M. Jemimah Carmichael, B. Nithya, and M. P. Sureshkumar, "Beam–column joint: structural behaviour using hybrid fibres," *Materials Today: Proceedings*, vol. 80, Part 3, pp. 3189–3192, 2023.

[30] A. Y. Ali and A. A. Al-Rammahi, "Flexural behavior of hybrid-reinforced concrete exterior beam–column joints under static and cyclic loads," *Fibres*, vol. 7, no. 10, Article ID 94, 2019.

[31] A. Nafees, M. F. Javed, M. A. Musarat, M. Ali, F. Aslam, and N. I. Vatin, "FE modelling and analysis of beam column joint using reactive powder concrete," *Crystals*, vol. 11, no. 11, Article ID 1372, 2021.

[32] A. B. Ugale and S. N. Khante, "Role of different types of varying hoops reinforcement in RC beam–column joint performance," *Materials Today: Proceedings*, vol. 27, Part 2, pp. 1590–1595, 2020.

[33] A. B. Ugale and S. N. Khante, "Study of energy dissipation of reinforced concrete beam–column joint confined using varying types of lateral reinforcements," *Materials Today: Proceedings*, vol. 27, Part 2, pp. 1356–1361, 2020.

[34] Bureau of Indian Standards, "IS 2386-3: methods of test for aggregates for concrete, part 3: specific gravity, density, voids, absorption and bulking," 1963.

[35] Bureau of Indian Standards, "IS 4031-6: methods of physical tests for hydraulic cement, part 6: determination of compressive strength of hydraulic cement (other than masonry cement)," 1988.

[36] A. Richardson and C. Galloway, "External para-aramid fibre–concrete reinforcement," *Structural Survey*, vol. 30, no. 2, pp. 163–173, 2012.

[37] M. A. Najafgholipour, S. M. Dehghan, A. Dooshabi, and A. Niroomandi, "Finite element analysis of reinforced concrete beam–column connections with governing joint shear failure mode," *Latin American Journal of Solids and Structures*, vol. 14, no. 7, pp. 1200–1225, 2017.

[38] X. Long and C. K. Lee, "Modelling of two dimensional reinforced concrete beam–column joints subjected to monotonic loading," *Advances in Structural Engineering*, vol. 18, no. 9, pp. 1461–1474, 2015.